Compaction-driven evolution of Pluto's rocky core: Implications for water-rock interactions.

Leila Gabasova[1], Gabriel Tobie[2] and Gaël Choblet[2], [1]IPAG, University of Grenoble, France (leila.gabasova@univ-grenoble-alpes.fr) and [2]LPG, University of Nantes, France

Introduction: Indirect evidence suggests that Pluto possesses an internal ocean [1], possibly interacting with the rocky core during billions of years. In order to assess the evolution of this ocean and the possibility of water-rock interactions, we revisit the thermal evolution of Pluto's interior by modeling the porosity evolution of the rocky core subsequent to accretion and by parameterizing the effect of porous circulation on heat transfer.

By exploring various initial porosity values and rheological properties of the rocky core, we determine the evolution of the porous layer, the vigor of water-rock interactions and the consequences for core cooling. We are also able to examine the effect of core evolution on the persistence of a liquid ocean beneath the outer ice shell, including the sensitivity to varying properties intrinsic to the ice shell.

Model: To model core compaction, we use a unified nonlinear viscoelastoplastic compaction model for saturated porous materials as defined by [2]. This model describes the possible range of the material's rheological responses to stress, from linear viscoelastic deformation at low temperatures and stress levels, going through intermediate viscoplastic cases, to full plastic compaction, and presents a set of incremental porosity evolution equations that covers all these cases. The input parameters are (1) the effective pressure, a function of the solid pressure in the matrix, the fluid pressure in the pores (assumed lithostatic and hydrostatic respectively), and the porosity, (2) the yield strength of the matrix, which we model empirically as a function of porosity and type of material, and (3) the effective viscosity of the rock, which we model based on its creep rate (assumed to have an Arrhenius dependence on temperature). Due to a lack of empirical silicate creep rate parameters for low-temperature conditions, we also set a maximum silicate viscosity threshold $\max(\eta_{sil})$ with a wide range of possible values.

With the compaction rate over time established, we parameterize the fluid convection within the porous layer of the core as an effective thermal conductivity, combining the real thermal conductivity of the matrix and of the fluid with heat transport via advection of the fluid. First, we express the permeability of the silicate matrix (modeled as a packed bed of spherical grains of diameter d_s) as a function of porosity. We then connect the flow's thermal Peclet number to the matrix permeability and the pressure gradient via Darcy's law. Finally, we implement an empirical expression for the effective thermal conductivity k_{hydro}, combining (a) the matrix thermal conductivity and (b) the fluid thermal conductivity and the thermal Peclet number, weighted by the porosity. The thermal evolution of the rocky core is then solved using the Crank-Nicholson method [3].

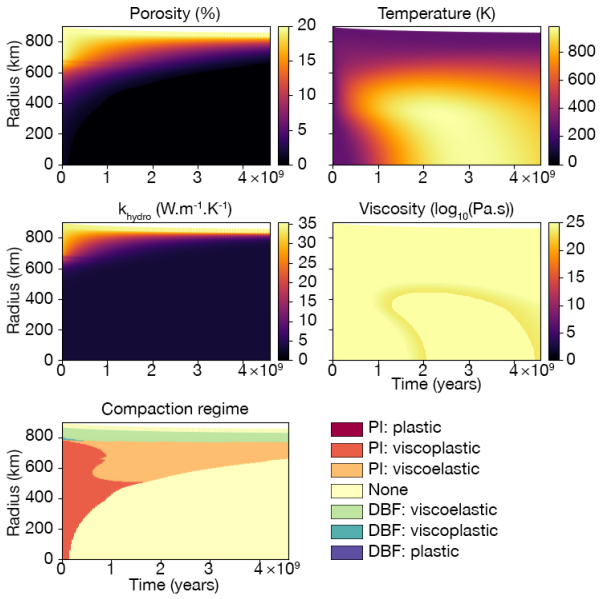

Figure 1: Core temporal cross-section for $\phi_0 = 0.2$, $\max(\eta_{sil}) = 10^{25}$ Pa.s, $d_s = 5$ mm.

Having established the core evolution model, we couple it with a pre-existing ice mantle evolution model [4, 5], initially developed for Titan, and adapted here to Pluto. It takes as input from the core model the heat flux, the core radius and the core mass, and also depends on the initial ice thickness, the reference melting point viscosity of the ice η_m and the initial ammonia concentration in the ocean $x_{NH_{3_0}}$. The mantle is modeled in a stagnant lid regime with an upper conductive ice layer atop convective ice.

Results: The nominal case for the core model is $d_s = 5$ mm, $\phi_0 = 0.2$, $\max(\eta_{sil}) = 10^{25}$ Pa.s, and yield strength parameters corresponding to a tuff-like material. Fig. 1 shows cross-sections representing the evolution over time of the porosity, temperature, equivalent thermal conductivity, effective silicate viscosity and compaction regime for this case.

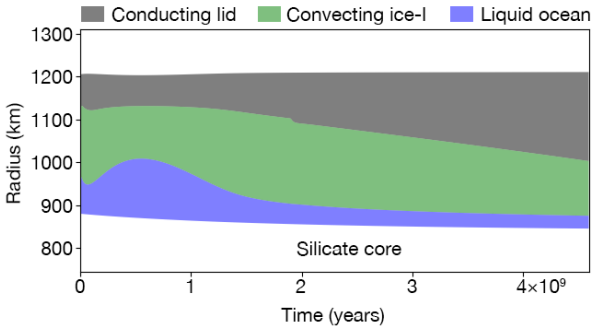

Figure 2: Mantle temporal cross-section nominal silicate core values, $x_{NH_{3_0}} = 1\%$, $\eta_{melt} = 10^{15}$ Pa.s.

We can see that in the nominal case the inner core undergoes very rapid viscoplastic compaction, with about 40% of the initial radius completely compacted by 1 Gy. The thickness of the outer porous layer decreases gradually in a viscoelastic compaction mode, constituting approximately 12-15% of the original radius at the present time (4.6 Gy).

Both decreasing and increasing the initial porosity leads to earlier cutoff of hydrothermal circulation (due to faster compaction for $\phi_0 = 0.1$ and a lower yield strength for $\phi_0 = 0.3$). The silicate viscosity threshold is a strong control for the compaction regime: a threshold of 10^{23} Pa.s results in immediate plastic compaction across all but the topmost layer, while one of 10^{27} Pa.s means that while the inner core still undergoes rapid collapse, the compaction in the outer core is insignificant even across multiple Gy. Via this effect on compaction, the viscosity threshold also strongly controls the maximal temperature. The grain size d_s does not directly affect the compaction rate, but as the equivalent hydrothermal conductivity k_{hydro} varies with d_s^3, varying d_s has a dramatic effect on heat flux and heat retention (e.g., $d_s =$ 1 mm effectively stops hydrothermal circulation). The type of material chosen for the yield strength calculation directly controls the threshold between compaction regimes, and thus the speed of compaction (e.g. a sandstone-like core compacts more plastically and thus faster than a tuff-like one).

Fig. 2 shows a temporal cross-section of the evolution of the mantle with nominal core parameters, $x_{NH_{3_0}} = 1\%$ and $\eta_{melt} = 10^{15}$ Pa.s. The liquid ocean's thickness is maximal at approximately 0.6-0.8 Gy, measuring roughly 100 km. It then decreases for about 1 Gy before stabilizing at a thickness of 20 km for the rest of the simulation. The conductive ice lid is thinnest when the ocean is maximal, and increases linearly thereafter, approaching 200 km by the end of the timeline.

While the range of parameters studied results in extremely different evolution timelines for the core, in most of these timelines a liquid ocean persists to the present day. The initial concentration of ammonia in the ocean is critical to its thickness and persistence over time, as established in earlier works [6]. Of the important core parameters, the maximum silicate viscosity threshold also strongly affects the mantle evolution, but the grain size is only critical for the early evolution stages (while the outer porous layer of the core is thick enough for hydrothermal circulation to take place).

Discussion: This is the first model for Pluto to feature compaction and hydrothermal circulation in the core, providing key constraints on the vigor of water-rock interactions through time. However, the model relies on multiple poorly constrained parameters, including the mineralogical composition of the core (which affects its yield strength) and the variation of its viscosity with temperature. Despite these uncertainties, by considering a wide range of rheological parameters we provide an array of possible timelines for the core's evolution.

A general outcome of our simulations is that a thick porous layer can exist in the outer part of the core during the first hundred millions of years, stimulating intense water-rock interactions. Interestingly, this time period coincides with the period of tidal dual synchronization of the Pluto-Charon system [7, 8]. Strong tidal heating is expected during Pluto's despinning, possibly powering hydrothermal activities similar to what is predicted in Enceladus [9]. A similar process is also expected inside Charon. The co-evolution of Pluto and Charon shortly after their formation event will be addressed in the near future.

References: **[1]** F. Nimmo et al. *Nature*, 540(7631):94, 2016. **[2]** V. M. Yarushina and Y. Y. Podladchikov. *J Geophys Res Solid Earth*, 120(6):4146–4170, 2015. **[3]** G. Tobie et al. *J Geophys Res Planets*, 108(E11), 2003. (Appendix A). **[4]** G. Tobie et al. *Icarus*, 175(2):496–502, 2005. **[5]** G. Tobie et al. *Nature*, 440(7080):61–64, 2006. **[6]** H. Hussmann et al. *Icarus*, 185(1):258–273, 2006. **[7]** A. C. Barr and G. C. Collins. *Icarus*, 246:146–155, 2015. **[8]** A. R. Rhoden et al. *Icarus*, 246:11–20, 2015. **[9]** G. Choblet et al. *Nature Astronomy*, 1(12):841, 2017.